Geo-Mar Lett
DOI 10.1007/s00367-016-0474-2

ORIGINAL

Observations of pockmark flow structure in Belfast Bay, Maine, Part 3: implications for sediment transport

Christina L. Fandel[1,2] · **Thomas C. Lippmann**[1] · **Diane L. Foster**[1] · **Laura L. Brothers**[3]

Received: 5 April 2016 / Accepted: 25 September 2016

Abstract Current observations and sediment characteristics acquired within and along the rim of two pockmarks in Belfast Bay, Maine, were used to characterize periods of sediment transport and to investigate conditions favorable to the settling of suspended sediment. Hourly averaged Shields parameters determined from horizontal current velocity profiles within the center of each pockmark never exceed the critical value (approximated with the theoretical model of Dade et al. 1992). However, Shields parameters estimated at the pockmark rims periodically exceed the critical value, consistent with conditions that support the onset of sediment transport and suspension. Below the rim in the near-center of each pockmark, depth-averaged vertical velocities were less than zero (downward) 60% and 55% of the time in the northern and southern pockmarks, and were often comparable to depth-averaged horizontal velocities. Along the rim, depth-averaged vertical velocities over the lower 8 m of the water column were primarily downward but much less than depth-averaged horizontal velocities indicating that suspended sediment may be moved to distant locations. Maximum grain sizes capable of remaining in suspension under terminal settling flow conditions (ranging 10–170 μm) were typically much greater than the observed median grain diameter (about 7 μm) at the bed. During upwelling flow within the pockmarks, and in the absence of flocculation, suspended sediment would not settle. The greater frequency of predicted periods of sediment transport along the rim of the southern pockmark is consistent with pockmark morphology in Belfast Bay, which transitions from more spherical to more elongated toward the south, suggesting near-bed sediment transport may contribute to post-formation pockmark evolution during typical conditions in Belfast Bay.

✉ Thomas C. Lippmann
lippmann@ccom.unh.edu

[1] Center for Coastal and Ocean Mapping, University of New Hampshire, 24 Colovos Rd., Durham, NH 03824, USA

[2] Hydrographic Surveys Division, Office of Coast Survey, National Oceanic and Atmospheric Administration, 1315 East-West Hwy, Silver Spring, MD 20910, USA

[3] U.S. Geological Survey, 384 Woods Hole Rd., Woods Hole, MA 02543, USA

Introduction

Belfast Bay is located in the northwestern Gulf of Maine, approximately 20 km southwest of the Penobscot River (346 m^3/s^2 mean discharge; PEARL 2011) and is characterized as a shallow, estuarine environment. The bay consists of over 1,750 pockmarks with a mean pockmark depth of 7.6 m and mean diameter of 84.8 m (Andrews et al. 2010). Sediment core data obtained by Brothers (2010) in Belfast Bay show inconsistent ages and radionuclide signatures as well as low sediment strength in the surface sediments. These observations suggest Belfast Bay is not described by an environment with steady sedimentation rates and that the existing sediment is frequently reworked.

The morphology of the pockmarks in Belfast Bay varies from more circular in the north to more elongated in the south where the bay constricts in width from 8.5 km to 2.6 km. Past expulsion of biogenetically derived methane is often invoked as the primary mechanism of pockmark formation in Belfast Bay, yet the present degassing activity remains unresolved (Brothers et al. 2012). Observations of acoustic backscatter (Brothers et al. 2011a), sidewall angles in excess of the angle of repose (Brothers et al. 2011b), and material being ejected from a pockmark (Kelley et al. 1994) provide evidence

Published online: 04 October 2016

consistent with actively degassing pockmarks in Belfast Bay. However, a recent geochemical survey of Belfast Bay reported no evidence of active methane or pore-fluid excavation and concluded that the Belfast Bay pockmarks may be inactive (Ussler et al. 2003; Brothers et al. 2011a). A recent presence/absence analysis of the Belfast Bay pockmarks indicated no change in macro-scale (>5 m) pockmark frequency or distribution between the years 1999 and 2008, and suggests that pockmarks can be maintained in environments with minimal fluid venting. Pockmarks found in low current velocity settings with an absence of fluid escape may be expected to fill in over time. However, many pockmarks that exist in these types of environments remain unfilled with maintenance mechanisms often attributed to flow-induced turbulence or low sedimentation rates (e.g., Hammer et al. 2009; Pau et al. 2014).

Current observations acquired by Manley et al. (2004) in the center of a pockmark in Lake Champlain, USA/Canada support the formation of a cyclostrophic rotational flow within the depression that could result in a limited deposition of fine-grained material. Using current measurements acquired in pockmarks located in Oslofjord, Norway and numerical modeling of flow over similar depressions, Hammer et al. (2009) also concluded that suspended sediment may not be capable of settling due to strong upward-directed vertical velocities within these depressions. Scaled-up water tank experiments completed by Pau et al. (2014) corroborated this conclusion and showed that downstream upwelling within the pockmark was sufficient to prevent the settling of very fine sand and enhanced turbulence within the depression was capable of supporting suspended material, which could subsequently be transported away from the pockmark. Additional sediment and acoustic backscatter data acquired within a pockmark in Oslofjord, Norway by Pau and Hammer (2013) suggest that pockmarks may be maintained by the resuspension of fine-grained material through current flow and biological activity in environments with minimal coarse-grain sediment input. Brothers et al. (2011b) examined uni-direction flow over a pockmark of similar geometry to those found in Belfast Bay through numerical modeling and small-scale flume tank experiments. They observed enhanced turbulence along the rim and base of the depression, which they suggest may foster an erosional feedback loop and modify pockmark morphology over time.

Recent field observations obtained in estuarine pockmarks located in Belfast Bay, Maine, show that strong overturning events extending from the rim to the bottom of the pockmark occur periodically (Part 1 companion paper, Fandel et al. 2016a), and that horizontal circulation and shear layer thickness evolution across the pockmark are qualitatively consistent with open cavity flow (Part 2, Fandel et al. 2016b). These observations suggest that near-bed turbulence induced by bottom shear stresses and circulation in the pockmark may lead to net sediment transport and contribute to morphologic evolution and long-term maintenance of pockmarks in Belfast Bay.

The present study examines hydrodynamic processes and sediment properties within and around two pockmarks in Belfast Bay using field observations of water velocities and sediment characteristics obtained within the center and along the rim of these depressions during a rising spring tide. The aim of this paper is to elucidate whether flow-induced stress may act in conjunction with, or in the absence of, natural gas and pore-water excavation to modify or maintain the Belfast Bay pockmark morphology.

Materials and methods

Sediment transport theory

Sediment transport of unconsolidated sediments on the seafloor is often parameterized by the Shields parameter, θ, defined as the balance between the fluid stresses mobilizing the sediment relative to the immersed weight of the grains, and given by

$$\theta = \frac{\rho u_*^2}{(\rho_s - \rho) g d_{50}} \tag{1}$$

where ρ is the density of water, ρ_s is sediment density, g is gravity, d_{50} is the median grain diameter, and u_* is the friction velocity. The Shields parameter characterizes the ratio of the bed shear stress applied over a single layer of sediment grains, $\tau_b = \rho u_*^2$, to the immersed weight of the sediment, $(\rho - \rho_s) g d_{50}$. Although there are noted inconsistencies (Buffington 1999) and experimental discrepancies (Shvidchenko and Pender 2000) with the work of Shields (1936), it is the most commonly used method to predict sediment transport (van Rijn 1993; Houwing and van Rijn 1998).

Under turbulent flow conditions, as observed over the sampled pockmarks (Part 1, Fandel et al. 2016a), the horizontal velocity profile can be characterized with a logarithmic model and a friction velocity estimated. The particle Reynolds number at the boundary, $u_* k_s / \upsilon$ where υ is the kinematic viscosity of water and $k_s = 2.5 d_{50}$ is the Nikuradse roughness, was less than 1 (with $d_{50} = 7$ μm; Table 1), and consequently hydrodynamic flow conditions are assumed. Following Whitehouse et al. (2000), under hydrodynamically smooth flow conditions, as are typically found in muddy estuaries (with $d_{50} <$ 62.5 μm) like Belfast Bay, the logarithmic velocity profile is a function of the water column shear given by

$$\frac{U(z)}{u_*} = 5.5 + 2.5 \ln\left(\frac{u_* z}{\upsilon}\right), \quad \frac{u_* k_s}{\upsilon} \leq 5 \tag{2}$$

where $U(z)$ is the mean horizontal velocity at height z. In this effort, $U(z)$ is taken as the resultant horizontal velocity composed of along- and across-pockmark flow. Estimates of u_* can be obtained from Eq. 2 through iteration and from logarithmic fits to values of $U(z)$ near the seabed.Shields (1936)

Table 1 Estimates of relative water content (M), yield stress (τ_y), median grain diameter (d_{50}) and critical Shields parameter (θ_{cr}) at the rim and center of each pockmark

		M (%)	τ_y (N/m^2)	d_{50} (μm)	θ_{cr}
Northern pockmark	Rim	155.64±1.06	2.88±0.03	7.65	0.19±0.001
	Center	154.89±0.98	2.90±0.01	7.28	0.20±0.001
Southern pockmark	Rim	167.56±4.27	2.67±0.08	7.06	0.19±0.004
	Center	212.35±30.11	1.84±0.56	6.33	0.15±0.04

Uncertainty measurements represent the range of variability observed between relative water content values from sediment obtained at the same location

characterizes the onset of sediment transport as the moment when the Shields parameter exceeds a critical value, θ_{cr}:

$$\theta_{cr} = \frac{\rho u_{*cr}^2}{(\rho_s - \rho) g d_{50}} \tag{3}$$

where u_{*cr} is a corresponding critical friction velocity. When sediment exhibits cohesive properties, the critical Shields parameter must account for the cohesive bonds between individual sediment grains. In the model for cohesive sediment by Dade et al. (1992), the critical Shields parameter is a function of the gravitational, frictional, and cohesive properties acting to keep a grain stationary in the presence of lift and drag forces imposed by the overriding, near-bed flow. In their model, the cohesive force between particles per grain surface area is represented by the yield stress, which has been empirically correlated to the critical bed shear stress by Mignoit (1968). Assuming the viscous region of the overriding turbulent flow is large relative to the spherical grain size, Dade et al. (1992) showed that the critical Shields parameter for mud may be approximated for grain roughness Reynolds number, Re_*, less than 3 by

$$\theta_{cr} = \frac{\frac{\pi}{b_1 48}\tan(\phi)}{1 + 0.1(\mathrm{Re}_*)_{cr}\tan(\phi)}\left(1 + \frac{F_A}{F_S}\right), \quad \mathrm{Re}_* < 3 \tag{4}$$

where φ is the angle of repose (or bed packing angle) approximated as 20°, typical of fine-grained marine sediment (Booth et al. 1985),

$$b_1 = \frac{\sqrt{1-R^2}}{R^{1/3}\cos^{-1}R}$$

$$\frac{F_A}{F_S} = 3b_2(1-\cos\phi)\frac{\tau_y}{(\rho_s-\rho)gd_{50}}$$

$$b_2 = \left(\frac{R}{18}\right)^{1/3}\left(2 + \frac{1}{R}\right)$$

and where the critical grain roughness Reynolds number is given by

$$(\mathrm{Re}_*)_{cr} = \frac{(u_*)_{cr} d_{50}}{\upsilon} \tag{5}$$

Summarizing Dade et al. (1992), the shape factor b_1 relates the drag force acting on the particle relative to the drag force acting on a sphere of equivalent volume, under the assumption that R, the characteristic aspect ratio of cylindrical grains, is less than one. The characteristic aspect ratio (R=0.8) was estimated from scanning electron microscope images of sediment collected in the western Gulf of Maine by Mazzullo et al. (1988). The shape factor b_2 is also a function of the characteristic aspect ratio, R, and accounts for the platiness of the particle. The ratio F_A/F_g relates the net interparticle cohesive force acting in the vertical (F_A) to the submerged particle weight induced by gravity (F_g), and is a function of the yield stress, τ_y, of the surficial fine-grained sediment. The yield stress of remolded sediment is typically and most directly measured using a controlled stress rheometer (Van Kessel and Blom 2012), and was empirically related to the measured moisture content of the soil, M, by Hoepner (2001):

$$\tau_y = 5.75 - 1.84M \tag{6}$$

Substitution of Eq. 5 into Eq. 4 and using Eqs. 3–6 yields a cubic equation in u_{*cr} that can be solved analytically, with the single real root being the solution of interest. The critical friction velocity can then be substituted into Eq. 3 to yield the critical Shields parameter that defines a threshold over which cohesive sediment is expected to move.

For sediment to settle out of suspension, the sediment settling velocity must be greater than the depth-averaged vertical velocities, W, near the bed. When depth-averaged vertical velocities are downward, all suspended sediment will eventually settle (and at a rate that varies with sediment grain size and density). Conversely, when depth-averaged vertical velocities are positive (upward), settling will only occur if the settling velocity of an individual particle is greater than the upwelling velocities. The terminal settling velocity of a particle is reached when the downward force induced by gravity is counteracted by the resistive force induced by the fluid's drag. Stokes' law (Winterwerp and Van Kesteren 2004) defines the terminal settling velocity, V_s, in terms of the particle diameter, d_n:

$$V_s = \frac{(\rho_s - \rho) g d_n^2}{18\mu} \tag{7}$$

where μ is the dynamic viscosity of water. The critical diameter, d_c, denotes the maximum grain diameter capable of remaining in suspension under the observed flow conditions and can

be determined by substituting the observed depth-averaged vertical velocities, W, for the terminal settling velocity, V_s, and solving for d_c such that

$$d_c = \sqrt{\frac{18W\mu}{(\rho_s - \rho)g}} \tag{8}$$

Comparison of d_c to the grain diameter, d_n, characterized by the observed median grain size, d_{50}, of the bed sediment provides some indication of whether suspended sediment grains would be expected to settle out in the presence of the observed vertical velocities.

It should be noted that Eq. 8 was developed for non-cohesive sediments, and does not account for fine-grained sediment deposition through flocculation. The degree of flocculation is controlled by a variety of sediment and flow characteristics including the size, concentration, organic matter content, and chemical properties of the suspended material, as well as the dimensions of the smallest turbulent eddies within the flow (Eisma 1986; van Leussen 1988; Manning et al. 2011). When depth-averaged vertical velocities are positive (upwelling conditions), the likelihood of unconsolidated sediment settling out of suspension can be qualitatively evaluated by estimating d_c from Eq. 8 and comparing these values to the observed d_{50}, providing at least a lower limit to expected settling behavior.

The theoretical development above indicates that estimation of the critical Shields parameter and maximum grain size under terminal settling conditions requires observation of the local hourly averaged horizontal current profiles, $U(z)$, hourly and depth-averaged vertical currents, W, and sediment characteristics, M and d_{50}.

Observations

The profile of the horizontal and vertical currents as well as sediment grain size distribution and relative water content were measured at the rim and center of two pockmarks in Belfast Bay to characterize periods of sediment transport and settling over a 48 h sampling period in late July 2011. Details of the acoustic Doppler current profiler (ADCP) deployments, pockmark geometry, and survey methods are described in Part 1 (Fandel et al. 2016a). Observations considered in this paper focus on the horizontal and vertical velocities averaged over the mid-water column, from 8 m below the water surface to the rim depth, and the deep-water column, from the rim depth to the bottom of the pockmark, and have accuracies of better than 0.0025 m/s (RD Instruments 2005; Fandel et al. 2016a).

Sediment samples were obtained from the center and rim of each pockmark using a Shipek grab sampler and were placed in sealed, quart-sized plastic bags. After acquisition, samples were analyzed for water content and grain size. Relative water content was estimated by measuring the loss of mass between a wet, m_{wet}, and then oven-dried, m_{dry}, sample, following standard procedures (ASTM 2010). Water content measurements following ASTM (2010) do not account for previously soluble solids within a sample, such as salt, but the associated error from this contribution is expected to be small. Data are represented as a percentage of the sample's dry mass, such that $M = (m_{wet} - m_{dry}) / m_{dry}$. Prior to completing sediment grain size analyses, sediment samples were placed in 100 mL beakers filled with a 3% hydrogen peroxide solution for 60 days to decompose all organic matter, and then disaggregated using an ultrasonic disintegrator immediately before completing the grain size analysis. Particle size distribution was measured using the Beckman Coulter LS 13320 laser diffraction particle size analyzer at the Woods Hole Oceanographic Institution Reinhart Coastal Research Center.

Results

Sediment properties

Water content measurements were made from four sediment samples obtained at the rim and center locations of each pockmark (Table 1). Relative water content values ranged from 155–212% by weight and in three of four cases varied by less than 5% between the two samples obtained from the same location. Although a larger variation (about 30%) in water content was observed from samples obtained at the center of the southern pockmark, the fractional error is within about 15%. These measurements are comparable to values obtained by Hoepner (2001) from sediment with similar characteristics to the Belfast Bay sediment. Yield stress (τ_y) estimates were calculated from mean water content values at each location using Eq. 6, following Hoepner (2001), and are shown in Table 1.

Sediment grain size distribution was measured at both the rim and center of each pockmark, and is shown in Fig. 1 as a function of grain size (in μm) and percent volume frequency. Median grain size (d_{50}), shown in Table 1, ranged from 6.33–7.65 μm and is representative of fine silt. Sampled sediments are assumed to have density (ρ_s) of 2,173 kg/m^3 based on the average density measurements obtained by Gschwend and Hites (1981) at 2–4, 18–22, and 34–38 m below the bed in Sommes Sound, Mt. Desert Island, ME, about 45 km to the east. Total organic matter was not measured in this study.

Horizontal and vertical currents

Observed hourly and depth-averaged horizontal and vertical velocities are shown in Fig. 2 as a function of tidal phase at the rim and center of each pockmark. A geographic right-handed coordinate system is used to describe current observations in this paper, with vertical datum at mean sea level and z-

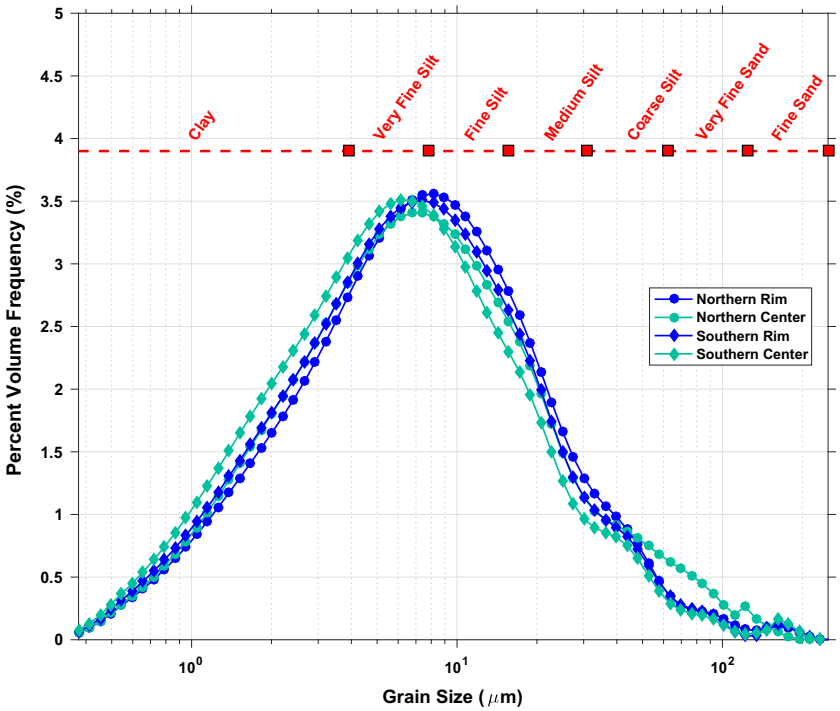

Fig. 1 Sediment distribution of samples collected at the rim (*blue*) and center (*teal*) of the northern (*circle*) and southern (*diamond*) pockmarks as a function of grain size and percent volume frequency. Grain size classification and delineation is according to Wentworth (1922)

coordinate positive upward. Water depths are reported as positive values. Mid-water flow (averaged between the rim and 8 m below the water surface) is strongly tidally modulated with maximum velocities occurring during mid-tidal phases. Horizontal mid-water currents are typically of the same order of magnitude during maximum flooding and ebbing tidal conditions and range from 0.03 to 0.17 m/s. Mid-water vertical velocities are nearly always downward, with maximum downwelling currents reaching –0.01 m/s. Upward vertical velocities are temporarily observed during maximum flooding tide, but do not exceed 0.005 m/s. Overall, mid-water column vertical velocities are downward 85% of the time and are

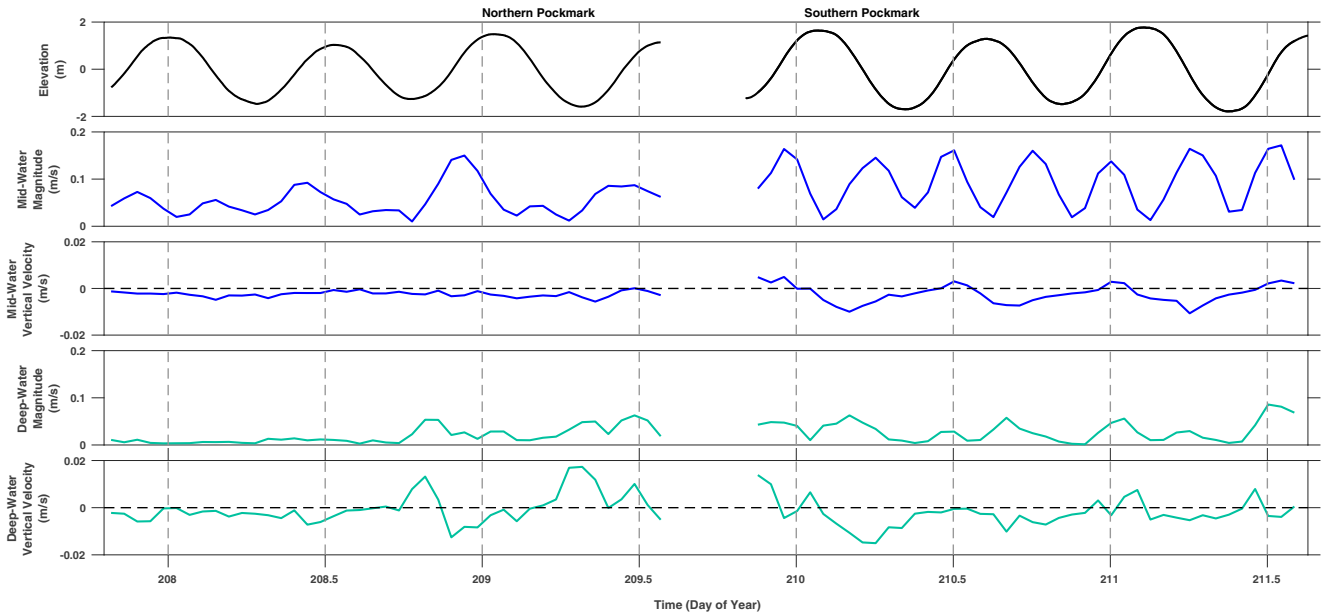

Fig. 2 Horizontal depth-averaged current magnitudes and vertical velocities observed at the rim (*teal*) and center (*blue*) of each pockmark with time (in days of year) on the x-axis. Rim currents are depth-averaged over the mid-water column from 8 m below the surface to the depth of the rim. Deep-water currents are depth-averaged from the rim depth to the bottom of the pockmark. *Upper panel* Mean sea surface elevation from bottom pressure data

consistently much less (by factors of 3–10 or more) than the corresponding depth-averaged horizontal velocities.

Depth-averaged horizontal velocities below the rim range in magnitude from 0.01–0.08 m/s and reach maximum velocities at mid-tidal phases. Compared to depth-averaged horizontal velocities above the rim, deep-water currents are weaker, a result of the nature of the flow within the pockmark (resembling and consistent with open cavity flow; Fandel et al. 2016b). Vertical velocities below the rim are comparable in magnitude to the deep-water horizontal flows and range from –0.02 to 0.02 m/s, with a tidally modulated pattern that shows periods of strong upwelling and downwelling (discussed in more detail in Part 1; Fandel et al. 2016a). Hourly averaged deep-water vertical velocities are downward 72% of the time during the northern pockmark sampling period and 81% of the time during the southern pockmark sampling period. This result is consistent with open cavity flow and a particular location of the ADCP within the pockmark (Fandel et al. 2016b).

The ratios of the hourly averaged vertical velocities, $w(z)$, to the corresponding hourly averaged horizontal current magnitudes $\left(\sqrt{u(z)^2+v(z)^2}\right)$ over the rim and center of each pockmark are shown in Fig. 3 as a function of depth. When $\left|\frac{w}{\sqrt{u^2+v^2}}\right| < 1$, the hourly averaged horizontal current magnitude is greater than the corresponding vertical velocities, and when $\left|\frac{w}{\sqrt{u^2+v^2}}\right| > 1$, the opposite is true. Overall, the ratio of the hourly averaged vertical velocities relative to the corresponding horizontal velocities increases and becomes more negative with depth. Above the rim, hourly averaged horizontal current magnitudes are typically much stronger than the corresponding vertical velocities, but decrease with depth. Below the rim, $\frac{w}{\sqrt{u^2+v^2}}$ becomes increasingly negative. Within about 10 m of the bed, vertical velocities are comparable in magnitude to the corresponding horizontal current velocities. Multiple hourly averaged periods are characterized by stronger depth-averaged vertical velocities relative to the corresponding horizontal flows below the rim. Although the mean flows do not dominate the system, they may have an impact on threshold levels.

It should be noted that the vertical to horizontal velocity ratio in the lowest bin of the center mounted ADCP in Fig. 3 was obtained from the Aquadopp acoustic current meter (see Fandel et al. 2016a). The observed inconsistency between current measurements made by the RDI Workhorse ADCP relative to the Aquadopp (closest, near-bed measurement) may be attributed to diminishing vertical velocities toward the seabed, different measurement parameters between the ADCP and Aquadopp (e.g., data averaging window, bin sampling frequency), and the potential influence of the instrument frame on the near-bottom currents that depends on the direction of the flow. An aspect that is not clear is the influence of

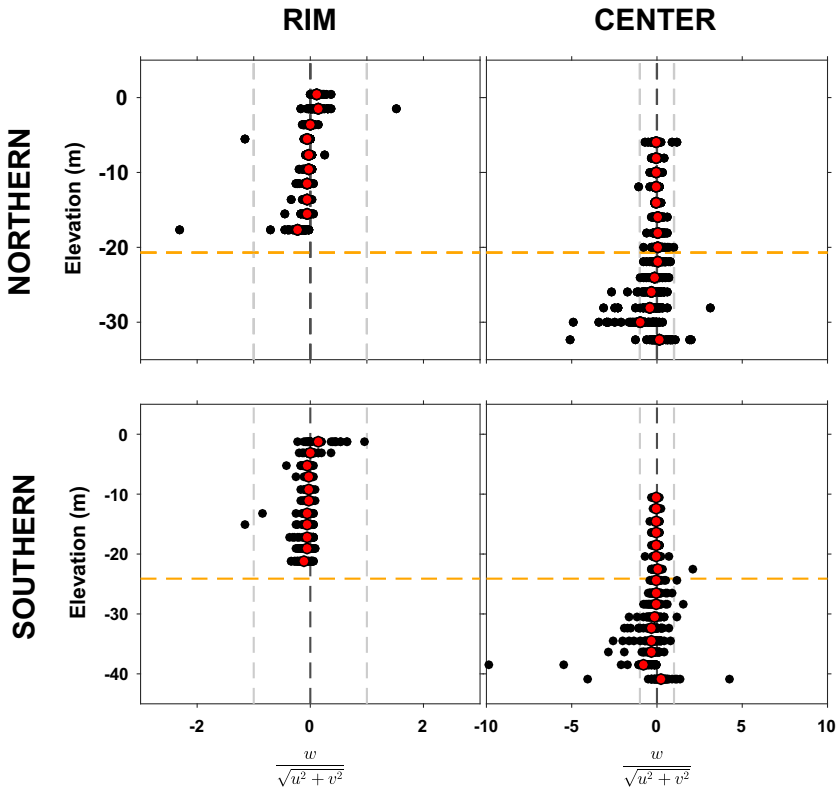

Fig. 3 Hourly averaged vertical velocities relative to horizontal current magnitudes as a function of depth over the rim (*left*) and center (*right*) of the northern (*upper*) and southern (*lower*) pockmark. *Black dots* Hourly averaged ratios of vertical velocities relative to horizontal current magnitudes at each depth, *red dots* mean values at each depth. The vertical dashed lines are at –1, 0, and 1 in each plot and are shown for horizontal scale (which varies between left and right panels). *Dashed orange line* Bottom of pockmark

the frame on the mean flows observed close to the bottom at an elevation of 7 cm above and about 30 cm to the side of the top of the frame (see Fandel et al. 2016a).

Sediment transport calculations

Hourly averaged friction velocities, u_*, were iteratively calculated using Eq. 2 and the observed hourly averaged horizontal velocity closest to the bed. In this case, the near-bed horizontal velocity was taken from the Aquadopp if it was consistent with a logarithmic profile defined by at least three data points (see Fandel et al. 2016a for details of the logarithmic fitting procedure); otherwise the lowest bin from the RDI Workhorse ADCP was used, with the same minimum data point requirements applied. These friction velocities are used in Eq. 1 to estimate the Shields parameters at both the rim and center positions of each pockmark. The estimated critical Shields parameter (θ_{cr}) was calculated using Eqs. 3–5 as a function of the measured d_{50} and τ_y. Estimated temporal evolution of critical (θ_{cr}) and hourly averaged Shields parameters (θ) at the rim and center of each pockmark are shown in Fig. 4. Estimates of θ_{cr} at each location are given in Table 1 with uncertainty based on the range of relative water content values obtained from the sampled sediment at each location. Estimates of θ at the rim exceed θ_{cr} several times on the rising and falling tides, approximately corresponding to periods of maximum flow. The critical Shields parameter is exceeded at the rim of the southern pockmark on five out of seven rising and falling tides, whereas at the rim of the northern pockmark θ_{cr} is only exceeded on one out of seven rising and falling tides. At the center current meter locations, θ is always much less than θ_{cr} and thus sediment transport is not expected to occur in the near-center of the pockmarks during the observed tidal flows.

The critical sediment grain diameter (d_c) is shown in Fig. 5 and denotes the maximum grain diameter capable of remaining in suspension given the observed positive mid-water and deep-water depth-averaged vertical velocities (W) at the ADCP locations on the rim and pockmark center, respectively. Average median grain diameter (d_{50} = 7.05 μm) is also shown in Fig. 5. When downward hourly averaged vertical velocities are observed, all grains are predicted to settle toward the bed irrespective of d_c (and hence d_c was not estimated during these periods). During upwelling events, estimated d_c was always much larger than the observed d_{50}, and suggests that in the absence of flocculation, all entrained grains less than the critical diameter (d_c) will remain in suspension.

Flocculation, unaccounted for in the analysis completed in this study, is expected to be strongly influenced by the flow regime and sediment characteristics (including organic matter) within Belfast Bay. Flocculation would result in larger sediment sizes and a concurrent increase in settling rates, particularly during prolonged periods of downwelling currents. As a consequence, effective in situ grain diameters of suspended material are most likely larger than the median grain diameter used herein, and suggests that a greater amount of sediment deposition would be expected in the vicinity of the observed pockmarks under similar flow conditions to those observed during this field experiment. Organic matter will undoubtedly influence the critical Shields parameter.

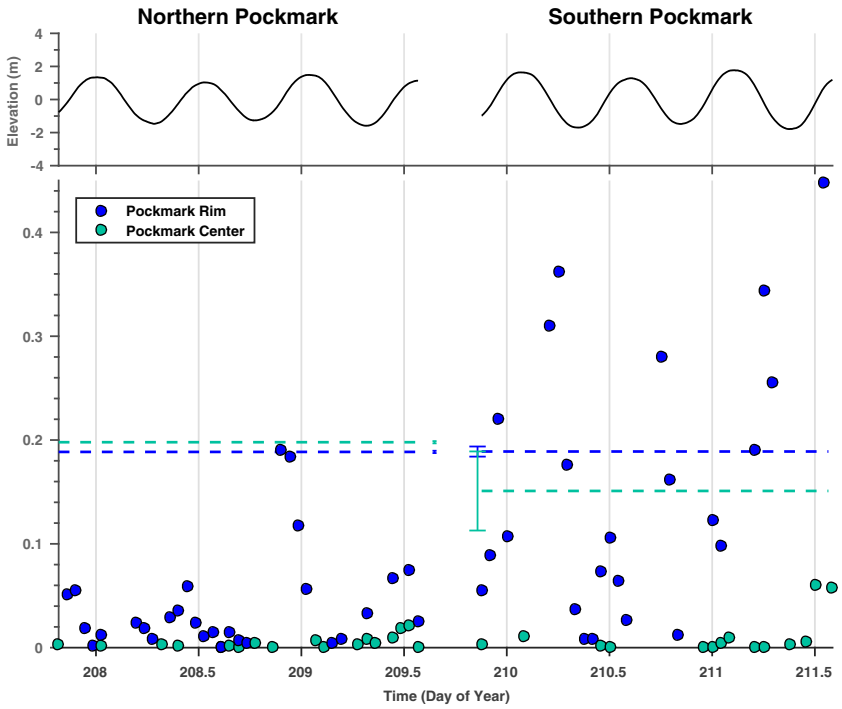

Fig. 4 Shields parameter estimates for each hourly averaged period at the rim (*blue*) and center (*teal*) of each pockmark as a function of time (*upper panel*). *Dashed lines* in the lower panel indicate the estimated critical Shields parameter with error bars representing the range based on observed variation in relative water content. Shields parameters were only estimated when a logarithmic profile was observed in the corresponding hourly averaged horizontal velocity profile (see Part 1; Fandel et al. 2016a)

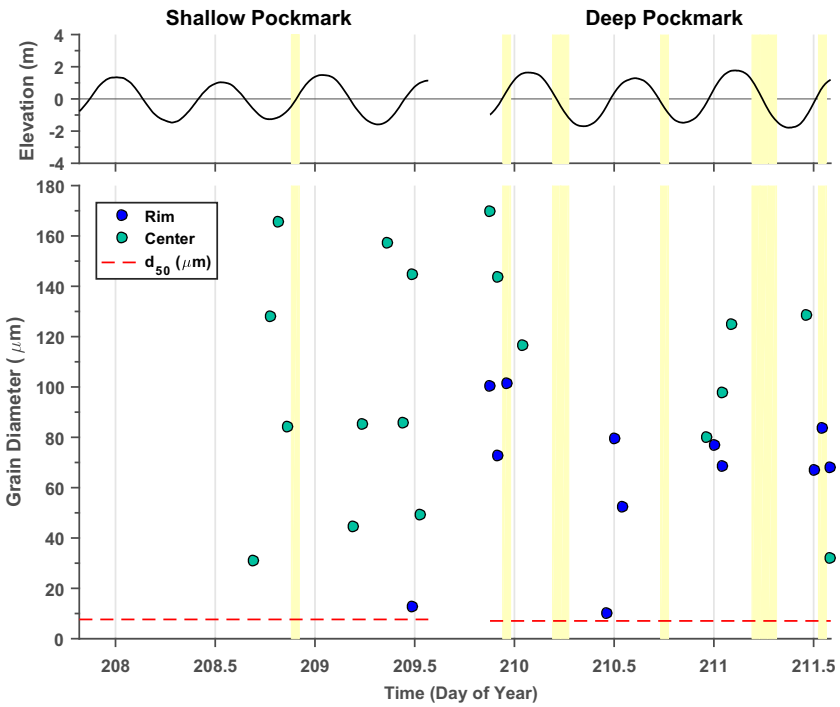

Fig. 5 Estimated maximum grain diameters predicted to remain in suspension during observed positive vertical velocity events at the rim (*blue*) and center (*teal*) of each pockmark as a function of time (*upper panel*). The *dashed red line* in the *lower panel* denotes the median grain diameter of 7.05 μm. Highlighted regions indicate periods during which sediment transport is predicted to occur. Note: critical diameter estimates under terminal settling conditions were calculated at the rim from positive depth-averaged mid-water vertical velocities and at the center from positive depth-averaged deep-water vertical velocities

Dade et al. (1992) approximate the influence of organic matter through the F_A term, via the yield stress of the sediment. Past studies have shown a positive correlation between the critical shear stress and organic content, and suggest theoretical approximations of the critical Shields parameter are often not accurate, and in situ field or laboratory tests should be used instead (e.g., Aberle et al. 2004).

Discussion

Sediment transport

Determining the critical threshold of erosion for cohesive sediment is difficult and is related to the physical, geochemical, and biological properties of the sediment and eroding fluid including the sediment concentration (Mignoit 1968), biogenic stabilization by benthic diatoms (Lundkvist et al. 2007), and water content (van Ledden et al. 2004). Because of the complexity in estimating the critical bed shear stress for cohesive sediments, laboratory tests using natural mud or in situ field tests are often employed. These tests preclude the treatment and storing of sediment, which often results in higher strength estimates than under natural settings. However, when in situ or laboratory tests cannot be achieved, the critical bed shear stress for cohesive sediments may be estimated following Dade et al. (1992), which incorporates the adhesive and cohesive properties of the sediment (e.g., interparticle cohesive bonding and organic binding) through measurement of the sediment's yield stress.

In this study, yield stress was estimated from a linear relationship to water content by Hoepner (2001). That model was developed empirically from comparison of measured yield stresses (obtained using a rheometer) and water content values measured from estuarine sediment samples similar in grain size and water content to the sampled Belfast Bay sediment. Differences in water content observed between two measurements obtained at the same location (rim or center) of either pockmark agree to within 15% error. Using the approximated sediment yield stress at each location, the critical Shields parameter was estimated following Dade et al. (1992) and the onset of sediment transport was predicted when $\theta > \theta_{cr}$ (Shields 1936). Estimated θ_{cr} is shown in Fig. 4 with error bars determined by the range in relative water content values, *M*. However, because estimated Shields parameters are often much greater than θ_{cr}, the general conclusions regarding sediment transport remain unchanged.

Estimates of θ along the rims of the northern and southern pockmarks are tidally modulated and greatest during the mid-tidal cycle periods (Fig. 4). The overall weaker, less tidally driven currents in the northern bay result in infrequent exceedance of the critical threshold for sediment transport along the rim. A more consistent pattern of critical threshold exceedance is observed along the rim of the southern pockmark where stronger tidal currents were observed. Although tidal currents are stronger during the flooding tide, maximum bed shear stresses along the rim more consistently occur during the ebbing flow. This asymmetry may be related to the local circulation pattern and relative location of the current meter mounts (northern rim) with respect to the primary tidal

direction. Field observations of pockmark rotational structure indicate flow reversal near the base of the pockmark and a greater degree of rotation during the ebbing tide, consistent with open cavity flow models (see Part 2, Fandel et al. 2016b). Stream-wise (horizontally varying) velocity structure over an open cavity predicts greater shear at the upstream edge of the cavity than at the downstream location. Thus, a greater bed stress would theoretically be expected during the ebbing tidal flow due to the location of the current meter mount on the northern rim of either pockmark.

The critical diameter under terminal settling conditions defines the largest grain diameter theoretically capable of remaining in suspension under the observed positive depth-averaged vertical velocities, and was always greater than the observed median grain diameter. This suggests that during periods when sediment transport is predicted to occur simultaneously with a strong upwelling event above the rim, it is possible that a significant fraction of non-flocculated sediment eroded from the rim of the pockmark would stay in suspension. Such events were recorded over two individual, hour-long periods at the rim of the southern pockmark and may characterize periods during which sediment remains in suspension. Conversely, simultaneous observations of predicted periods of sediment transport along the rim with downward-directed depth-averaged currents above the pockmark would characterize periods during which sediment settles toward the bed, and were observed 78% of the time during this sampling period. However, the ratio $w/\sqrt{u^2+v^2}$ over the rim negatively increases with depth and is rarely outside the range –1 to 1. Close to the bed at the rim, the flow structure, consistent with boundary layer theory, is primarily characterized by weak downward vertical velocities and stronger horizontal flows. As a result, when estimated periods of sediment transport occur simultaneously with downward-directed vertical velocities below the rim, suspended sediment may be transported downstream a distance before it is deposited. This ratio will have an impact on the mode of sediment transport (e.g., bedload or suspended load), and possibly on the friction velocity. At the bed, a relatively larger vertical velocity could result in a drop in the threshold of motion, but without additional measurements it is not possible to quantify the effect.

In the center of each pockmark, θ never exceeded θ_{cr}, and near-bed sediment transport is not expected to occur during these average tidal flows. Furthermore, deep-water vertical velocities, comparable in magnitude to the depth-averaged horizontal velocities below the rim, are less than zero (downwelling currents) 75% of the time. This suggests that—on average—suspended sediments in the water column would tend to settle toward the bed. However, observations over the center of the pockmark showing $w/\sqrt{u^2+v^2} > 1$ at various depths below the rim—in conjunction with estimated critical diameters much greater than the median grain diameter at the bed—suggest that any suspended sediment below the rim during these time periods may be kept in suspension for longer periods and transported up and out of the pockmark. Pau et al. (2014) also concluded that suspended sediment, kept in suspension by enhanced turbulence in the center of the depression, could be transported out of the pockmark by horizontal flow. Their scaled experimental measurements of fluid flow over pockmark geometry also show upwelling along the downstream edge of the depression strong enough to prevent the settling of fine sand. Similar results were obtained by Pau and Hammer (2013) from sediment and acoustic backscatter observations within a pockmark in the Oslofjord, Norway, which showed coarser sediment, enhanced turbulence and a greater amount of sediment resuspension near the pockmark center than outside the depression. Pau and Hammer (2013) suggest that the enhanced turbulence within the pockmark center may cause fines to stay in suspension and be subsequently transported away from the pockmark by currents, whereas coarser sediment, including flocculated material, may be transported as bedload and deposited. The results herein suggest bedload transport should be much less than suspended sediment in Belfast Bay; their observations are, in general, consistent with the observations made of sediment transport and settling conditions in this study, and suggest that pockmark suspended sediment transport patterns may be similar in different geographical regions.

Following Dade et al. (1992), the role of bed slope on the critical shear stress is ignored. The impacts of bed slope are (primarily) through the angle of repose of the sediment grains, which will decrease as bed slope increases. At the point when the angle of repose equals the bed slope, slope failure (or slumping) occurs. The critical Shields parameter (Eq. 1) depends on the angle of repose (in a complex way) but not directly on the bed slope. With all other parameters the same, the critical Shields parameter decreases with an increase in bed slope, allowing for more easily moved sediment grains and increasing the likelihood for sediment transport. Herein, the effects of slope are not considered and thus critical Shields parameters are likely overestimated where the slopes are steeper. Considering the uncertainties in actual value for the angle of repose, and by not including flocculation processes (which will promote sedimentation), the more conservative estimate for transport is retained.

It should be noted that the calculated Shields parameters and critical thresholds represent estimates of the likelihood of sediment transport occurring, and that motion may be occurring well before a critical threshold is reached. Figure 4 shows how the Shields parameter varies with time over each pockmark with estimated critical values indicated. Even if the critical values change by a factor of 2, the general behavior of the calculated Shields parameters shows that transport is more likely to be occurring more often at the rim of the southern pockmark. This observation is consistent with the elongation of the pockmark rim morphology.

A further complication is that the settling of grains through the water column will depend on the level of turbulent fluctuations that may serve to keep particles in suspension (Bagnold 1966; Kassem et al. 2015), regardless of their settling rates or time-averaged vertical velocity. As high-frequency observations of turbulent sweeps or bursts were not made in this study and the ADCP profile observations require averaging many pings to obtain the necessary resolution to resolve up- and downwelling currents, the specific role played by higher-frequency motions during the measurement period in initiating or maintaining pockmark suspension events is not addressed. As a consequence, it cannot be discounted that turbulent eddies have an impact on net transport patterns (a significant problem common to many sediment transport field applications). Pau et al. (2014) observed formation of turbulent eddies at the upstream edge of the pockmark that were subsequently advected by the current, providing some evidence that turbulence may act to keep sediment in suspension in pockmarks.

Pockmark morphology and maintenance

Pockmark morphology in Belfast Bay transitions from more spherical in the north to more elongated in the south and suggests that pockmark shape may not be exclusively controlled by vertical fluid circulation. Critical sediment grain diameter estimations under terminal settling velocity conditions in excess of the median grain diameter, together with observed periods of sediment transport along the rim of the southern pockmark, suggest that pockmark size and shape may be modified by local sediment transport. The greater frequency of excess bed shear stress along the rim of the more southerly located pockmark is consistent with the elongated morphology of the pockmarks in the southern region of Belfast Bay. Similar observations of pockmark morphology transitioning from spherical to more elongated with distance offshore are found in Blue Hill Bay, Maine, and Passamaquoddy Bay, New Brunswick, Canada (Brothers et al. 2012), and may be related to fine-grained sediment erosion induced by excess bed shear stress along the rims of the pockmarks. Elongated features are also observed in stratigraphic records in the North Sea and may be due to sediment transport patterns similar to ours by bottom currents on the shelf (Kilhams et al. 2011).

Although sediment transport is predicted along the rims of each pockmark, it is never predicted to occur at the near-center of the pockmarks (and it should be noted that sediment transport may have occurred prior to reaching a critical Shields value). Observations at the center of each pockmark of primarily negative (downward-directed) vertical velocities below the rim in conjunction with $\theta < \theta_{cr}$ for all data would result in pockmarks that fill in over time; yet these features have persisted for up to 11,000 years (Brothers 2010). Potential mechanisms to explain the preservation of these large depressions over long time periods could be related to bedload transport (important in Oslofjord; Pau and Hammer 2013), or to the influence of strong upwelling or local storm events that enhance sediment transport within pockmarks. Strong upwelling events below the rim, as observed in this study (Part 1; Fandel 2016a), may promote suspended sediment advection out of the pockmark and more or less balance the net sediment deposition occurring during downwelling periods below the rim. Alternately, pockmark maintenance may be primarily controlled by sediment transport induced by higher-velocity flow during spring tides or wind-driven currents, rather than during the average (benign) conditions that occurred during this sampling period.

Conclusions

Water velocities and sediment observations acquired at the rim and center of two pockmarks in Belfast Bay, ME were used to estimate periods of sediment transport and to assess whether or not suspended sediment in the water column would settle under the observed velocities. Results suggest that sediment transport regularly occurs during maximum flood and ebb tidal periods at the rim of each pockmark. Near-bed stress imposed by overriding currents within the pockmarks was not strong enough to exceed sediment transport thresholds (although it is possible that transport may have occurred well beforehand). Observations obtained at the rim of the pockmarks are consistent with suspended sediment being transported downstream to a distant location. Flow observations in the center of the pockmarks are consistent with a large portion of suspended sediment settling during downwelling periods. Although sediment characteristics suggest that sediment entrained into the flow would remain in suspension while the flow conditions persisted, the influence of flocculation is not accounted for in the analysis.

The more frequent occurrences when conditions favor sediment transport at the rim of the southern pockmark (rather than the northern pockmark) qualitatively agree with the observed pockmark morphology in Belfast Bay, which becomes more elongated with progression southward. However, the majority of observed currents are characterized by downward, depth-averaged vertical velocities, weak horizontal currents below the rim, and strong mid-water horizontal currents. This suggests that a large proportion of the sampling period is characterized by the settling of suspended sediment in the center of the pockmark (with or without flocculation). Long-term pockmark maintenance may therefore be related to a larger amount of sediment being transported out of the pockmark during upwelling periods than is deposited during downwelling periods (but is not verified from the data collected in this study).

Acknowledgments Data used in this study are available at the Center for Coastal and Ocean Mapping, University of New Hampshire under the experiment name "2011 Belfast Bay Pockmark Experiment". J. Kelley of the University of Maine provided the multibeam bathymetry map from which candidate pockmarks were identified for further study. This work was based upon a model conceived by P. Koons at the University of Maine and the many observations and interpretations made by J. Kelley, D. Belknap (University of Maine), W. Barnhardt (USGS), and B. Andrews (USGS). L. Giosan generously provided the use of the LS 13 230 Laser Diffraction Particle Size Analyzer at Woods Hole Oceanographic Institution. Field assistance was provided by J. Irish, Capt. E. Terry, Capt. B. Smith, and J. Hunt. Comments by J. Irish, D. Nowacki, and the anonymous reviewers greatly improved the manuscript. This research was supported by the National Oceanic and Atmospheric Administration under NOAA gran NA10NOS4000073. Any use of trade, firm, or product names is for descriptive purposes only and does not imply endorsement by the U.S. Government. Any use of trade, firm, or product names is for descriptive purposes only and does not imply endorsement by the U.S. Government.

Compliance with ethical standards

Conflict of interest The authors declare that there is no conflict of interest with third parties.

References

Aberle J, Nikora V, Walters R (2004) Effects of bed material properties on cohesive sediment erosion. Mar Geol 207:83–93

Andrews BD, Brothers LL, Barnhardt WA (2010) Automated feature extraction and spatial organization of seafloor pockmarks, Belfast Bay, Maine, USA. Geomorphology 124:55–64

ASTM (2010) Standard D2216-10. Standard test methods for laboratory determination of water (moisture) content of soil and rock by mass. ASTM International, West Conshohocken, PA

Bagnold RA (1966) An approach to the sediment transport problem from general physics. Physiographic and Hydraulic Studies of Rivers, Geological Survey Professional Paper 422-I

Booth JS, Sangrey D, Fugate J (1985) A nomogram for interpreting slope stability of fine-grained deposits in ancient and modern marine environments. J Sed Petrol 55:29–36

Brothers LL (2010) Nearshore pockmark field dynamics and evolution. PhD Dissertation, University of Maine, Orono, ME

Brothers LL, Kelley JT, Belknap DF, Barnhardt WA, Andrews BD, Maynard ML (2011a) More than a century of bathymetric observations and present-day shallow sediment characterization in Belfast Bay, Maine, USA: implications for pockmark field longevity. Geo-Mar Lett 31:237–248

Brothers LL, Kelley JT, Belknap DF, Barnhardt WA, Koons PO (2011b) Pockmarks: self-scouring seep features? In: Proc 7th Int Conf Gas Hydrates, 17–21 July, Edinburgh, UK

Brothers LL, Kelley JT, Belknap DF, Barnhardt WA, Andrews BD, Legere C, Hughes Clarke JE (2012) Shallow stratigraphic control on pockmark distribution in north temperate estuaries. Mar Geol 329–331:34–45

Buffington JM (1999) The legend of A.F. shields. J Hydraul Eng 125: 376–387

Dade WB, Nowell ARM, Jumars PA (1992) Predicting erosion resistance of muds. Mar Geol 105:285–297

Eisma D (1986) Flocculation and de-flocculation of suspended matter in estuaries. Neth J Sea Res 20:183–199

Fandel CL, Lippmann TC, Irish JD, Brothers LL (2016a) Observations of pockmark flow structure in Belfast Bay, Maine, Part 1: current-induced mixing. Geo-Mar Lett, this volume. doi:

Fandel CL, Lippmann TC, Foster DL, Brothers LL (2016b) Observations of pockmark flow structure in Belfast Bay, Maine, Part 2: evidence for cavity flow. Geo-Mar Lett, this volume. doi:

Gschwend PM, Hites RA (1981) Fluxes of polycyclic aromatic hydrocarbons to marine and lacustrine sediments in the northeastern United States. Geochim Cosmochim Acta 45:2359–2367

Hammer Ø, Webb KE, Depreiter D (2009) Numerical simulation of upwelling currents in pockmarks, and data from the Inner Oslofjord, Norway. Geo-Mar Lett 29:269–275

Hoepner MA (2001) Stability of cohesive sediments from flume and rheometer measurements. MS Thesis, Georgia Institute of Technology, Atlanta, GA

Houwing E-J, van Rijn LC (1998) In situ erosion flume (ISEF): determination of bed-shear stress and erosion of a kaolinite bed. J Sea Res 39:243–253

RD Instruments (2005) WorkHorse Monitor, Sentinel, Rio Grande, and Mariner Acoustic Doppler Current Profiler technical manual

Kassem H, Thompson CEL, Amos CL, Townend IH (2015) Wave-induced coherent turbulence structures and sediment resuspension in the nearshore of a prototype-scale sandy barrier beach. Cont Shelf Res 109:78–94

Kelley JT, Dickson SM, Belknap DF, Barnhardt WA, Henderson M (1994) Giant sea-bed pockmarks: evidence for gas escape from Belfast Bay. Geology 22:59–62

Kilhams B, McArthur A, Huuse M, Ita E, Hartley A (2011) Enigmatic large-scale furrows of Miocene to Pliocene age from the central North Sea: current-scoured pockmarks? Geo-Mar Lett 31:437–449

Lundkvist M, Grue M, Friend PL, Flindt MR (2007) The relative contributions of physical and microbiological factors to cohesive sediment stability. Cont Shelf Res 27:1143–1152

Manley PL, Manley TO, Watzin MC, Gutierrez J (2004) Lakebed pockmarks in Burlington Bay, Lake Champlain: I. hydrodynamics and implications of origin. In: Manley TO, Manley PL, Mihuc TB (eds) Lake Champlain: partnerships and research in the new millennium. Springer, Berlin, pp 299–330

Manning AJ, Baugh JV, Soulsby RL, Spearman JR, Whitehouse RJS (2011) Cohesive sediment flocculation and the application to settling flux modelling. In: Ginsberg SS (ed) Sediment transport. InTech, pp 91–116

Mazzullo J, Leschak P, Prusak D (1988) Sources and distribution of Late Quaternary silt in the surficial sediment of the northeastern continental shelf of the United States. Mar Geol 78:241–254

Mignoit C (1968) A study of the physical properties of various very fine sediments and their behavior under hydrodynamic action. Houille Blanche 23:591–620

Pau M, Hammer O (2013) Sediment mapping and long-term monitoring of currents and sediment fluxes in pockmarks in the Oslofjord, Norway. Mar Geol 346:262–273

Pau M, Gisler G, Hammer Ø (2014) Experimental investigation of the hydrodynamics in pockmarks using particle tracking velocimetry. Geo-Mar Lett 34:11–19

PEARL (2011) Penobscot River Synthesis. http://www.pearl.maine.edu/windows/penobscot/research_hydrology.htm

Shields A (1936) Anwendung der Aehnlichkeitsmechanik und Turbulenzforschung auf die Geschiebebewegung. Mitt Preuss Versuchsanstalt für Wasserbau und Schiffbau 26:1–26

Shvidchenko AB, Pender G (2000) Flume study of the effect of relative depth on incipient motion of coarse uniform sediments. Water Resour Res 36:619–628

Ussler W III, Paull CK, Boucher J, Friederich GE, Thomas DJ (2003) Submarine pockmarks: a case study from Belfast Bay, Maine. Mar Geol 202:175–192

Van Kessel T, Blom C (2012) Rheology of cohesive sediments: comparison between a natural and an artificial mud. J Hydraul Res 36:591–612

van Ledden M, van Kesteren WGM, Winterwerp JC (2004) A conceptual framework for the erosion behaviour of sand–mud mixtures. Cont Shelf Res 24:1–11

van Leussen W (1988) Aggregation of particles, settling velocity of mud flocs: a review. In: Dronkers J, Van Leussen W (eds) Physical processes of estuaries. Springer, Berlin, pp 347–403

van Rijn LC (1993) Principles of sediment transport in rivers, estuaries, and coastal seas. Aqua Publications, Amsterdam

Wentworth CK (1922) A scale of grade and class terms for clastic sediments. J Geol 30:377–392

Whitehouse R, Soulsby R, Roberts W, Mitchener H (2000) Dynamics of estuarine muds. Thomas Telford, London

Winterwerp JC, Van Kesteren WGM (2004) Introduction to the physics of cohesive sediment in the marine environment. Elsevier, Amsterdam